Resonant structure of $\tau \to 3\pi\pi^0\nu_\tau$ and $\tau \to \omega\pi\nu_\tau$ decays

K. W. Edwards
Carleton University, Ottawa, Ontario, Canada K1S 5B6
and the Institute of Particle Physics, Canada

R. Janicek and P. M. Patel
McGill University, Montréal, Québec, Canada H3A 2T8
and the Institute of Particle Physics, Canada

A. J. Sadoff
Ithaca College, Ithaca, New York 14850

R. Ammar, P. Baringer, A. Bean, D. Besson, R. Davis, S. Kotov, I. Kravchenko, N. Kwak, and X. Zhao
University of Kansas, Lawrence, Kansas 66045

S. Anderson, V. V. Frolov, Y. Kubota, S. J. Lee, R. Mahapatra, J. J. O'Neill, R. Poling, T. Riehle, and A. Smith
University of Minnesota, Minneapolis, Minnesota 55455

S. Ahmed, M. S. Alam, S. B. Athar, L. Jian, L. Ling, A. H. Mahmood,* M. Saleem, S. Timm, and F. Wappler
State University of New York at Albany, Albany, New York 12222

A. Anastassov, J. E. Duboscq, K. K. Gan, C. Gwon, T. Hart, K. Honscheid, H. Kagan, R. Kass, J. Lorenc, H. Schwarthoff, E. von Toerne, and M. M. Zoeller
Ohio State University, Columbus, Ohio 43210

S. J. Richichi, H. Severini, P. Skubic, and A. Undrus
University of Oklahoma, Norman, Oklahoma 73019

M. Bishai, S. Chen, J. Fast, J. W. Hinson, J. Lee, N. Menon, D. H. Miller, E. I. Shibata, and I. P. J. Shipsey
Purdue University, West Lafayette, Indiana 47907

Y. Kwon,† A. L. Lyon, and E. H. Thorndike
University of Rochester, Rochester, New York 14627

C. P. Jessop, K. Lingel, H. Marsiske, M. L. Perl, V. Savinov, D. Ugolini, and X. Zhou
Stanford Linear Accelerator Center, Stanford University, Stanford, California 94309

T. E. Coan, V. Fadeyev, I. Korolkov, Y. Maravin, I. Narsky, V. Shelkov, R. Stroynowski, J. Ye, and T. Wlodek
Southern Methodist University, Dallas, Texas 75275

M. Artuso, R. Ayad, E. Dambasuren, S. Kopp, G. Majumder, G. C. Moneti, R. Mountain, S. Schuh, T. Skwarnicki, S. Stone, A. Titov, G. Viehhauser, J. C. Wang, A. Wolf, and J. Wu
Syracuse University, Syracuse, New York 13244

S. E. Csorna, K. W. McLean, S. Marka, and Z. Xu
Vanderbilt University, Nashville, Tennessee 37235

R. Godang, K. Kinoshita,‡ I. C. Lai, P. Pomianowski, and S. Schrenk
Virginia Polytechnic Institute and State University, Blacksburg, Virginia 24061

G. Bonvicini, D. Cinabro, R. Greene, L. P. Perera, and G. J. Zhou
Wayne State University, Detroit, Michigan 48202

S. Chan, G. Eigen, E. Lipeles, M. Schmidtler, A. Shapiro, W. M. Sun, J. Urheim, A. J. Weinstein, and F. Würthwein
California Institute of Technology, Pasadena, California 91125

D. E. Jaffe, G. Masek, H. P. Paar, E. M. Potter, S. Prell, and V. Sharma
University of California, San Diego, La Jolla, California 92093

0556-2821/2000/61(7)/072003(16)/$15.00

D. M. Asner, A. Eppich, J. Gronberg, T. S. Hill, D. J. Lange, R. J. Morrison, T. K. Nelson, and J. D. Richman
University of California, Santa Barbara, California 93106

R. A. Briere
Carnegie Mellon University, Pittsburgh, Pennsylvania 15213

B. H. Behrens, W. T. Ford, A. Gritsan, H. Krieg, J. Roy, and J. G. Smith
University of Colorado, Boulder, Colorado 80309-0390

J. P. Alexander, R. Baker, C. Bebek, B. E. Berger, K. Berkelman, F. Blanc, V. Boisvert, D. G. Cassel, M. Dickson, P. S. Drell, K. M. Ecklund, R. Ehrlich, A. D. Foland, P. Gaidarev, R. S. Galik, L. Gibbons, B. Gittelman, S. W. Gray, D. L. Hartill, B. K. Heltsley, P. I. Hopman, C. D. Jones, D. L. Kreinick, T. Lee, Y. Liu, T. O. Meyer, N. B. Mistry, C. R. Ng, E. Nordberg, J. R. Patterson, D. Peterson, D. Riley, J. G. Thayer, P. G. Thies, B. Valant-Spaight, and A. Warburton
Cornell University, Ithaca, New York 14853

P. Avery, M. Lohner, C. Prescott, A. I. Rubiera, J. Yelton, and J. Zheng
University of Florida, Gainesville, Florida 32611

G. Brandenburg, A. Ershov, Y. S. Gao, D. Y.-J. Kim, and R. Wilson
Harvard University, Cambridge, Massachusetts 02138

T. E. Browder, Y. Li, J. L. Rodriguez, and H. Yamamoto
University of Hawaii at Manoa, Honolulu, Hawaii 96822

T. Bergfeld, B. I. Eisenstein, J. Ernst, G. E. Gladding, G. D.Gollin, R. M. Hans, E. Johnson, I. Karliner, M. A. Marsh, M. Palmer, C. Plager, C. Sedlack, M. Selen, J. J. Thaler, and J. Williams
University of Illinois, Urbana-Champaign, Illinois 61801

(CLEO Collaboration)

(Received 30 September 1999; published 8 March 2000)

The resonant structure of the four pion final state in the decay $\tau \to 3\pi\pi^0\nu_\tau$ has been analyzed using 4.27 million $\tau^+\tau^-$ pairs collected by the CLEO II experiment at the Cornell Electron Storage Ring. A partial wave analysis of the resonant structure of the $\tau \to 3\pi\pi^0\nu_\tau$ decay has been performed; the spectral decomposition of the four pion system is dominated by the $\omega\pi$ and $a_1\pi$ final states. The mass and width of the ρ' resonance have been extracted from a fit to the $\tau \to \omega\pi\nu_\tau$ spectral function. We have searched for second class currents in the decay $\tau \to \omega\pi\nu_\tau$ using spin-parity analysis and established an upper limit on the non-vector current contribution.

PACS number(s): 13.25.Jx, 13.35.Dx, 14.40.Cs, 14.60.Fg

I. INTRODUCTION

The resonant structure of the decay $\tau \to 4\pi\nu_\tau$ has been the subject of extensive experimental studies. The first observations of $\tau \to \omega\pi\nu_\tau$ were reported by the ARGUS [1] and the CLEO [2] Collaborations in 1987. Since then, the ARGUS Collaboration estimated [3] the $\rho\pi\pi$ branching fractions and the ALEPH Collaboration provided improved measurements [4] of branching fractions of the $\tau \to 4\pi\nu_\tau$ subchannels. No attempt has been made, so far, to determine a complete resonant structure of the four pion final state.

In the standard model, the τ decay to four pions proceeds via the vector current producing hadrons in the $J^P = 1^-$ spin-parity state. At low energies, the hadronic current is dominated by vector ρ, ρ', and ρ'' resonance form factors which can be approximated by relativistic Breit-Wigner functions. The full formalism is discussed in Refs. [5–8]. The decay can proceed via various subresonant states (e.g., $\omega\pi$, $a_1\pi$, $\rho\pi\pi$ etc.) whose contributions interfere with each other. The parameters of $J^P = 1^-$ resonances are of particular interest for phenomenological tests of the conserved vector current (CVC) hypothesis that compare multipion final states in τ decays and e^+e^- annihilations [9].

While the mass and width of the ρ have been well measured, the parameters of the ρ' resonance are known with a large uncertainty [10]. Most of the ρ' measurements are based on proton experiments on a fixed target and e^+e^- collisions. So far, there have been only two published attempts [11,12] to extract the mass and width of the ρ' reso-

*Permanent address: University of Texas - Pan American, Edinburg, TX 78539.

†Permanent address: Yonsei University, Seoul 120-749, Korea.

‡Permanent address: University of Cincinnati, Cincinnati, OH 45221.

nance from analyses of the $\tau \to \pi\pi^0\nu_\tau$ decay and none from $\tau \to 4\pi\nu_\tau$.

If G-parity conservation is broken, the decay $\tau \to \omega\pi\nu_\tau$ can be mediated by second class currents [13] producing pions in a different spin-parity state. In the previous study [4] ALEPH has searched for second class currents and set an upper limit on the non-vector current contribution. We repeat this analysis with larger statistics.

In this study, we determine the resonant decomposition of the decay $\tau \to \omega\pi\nu_\tau$ and search for second class currents via a spin-parity analysis. We fit the $\tau \to \omega\pi\nu_\tau$ spectral function to obtain the relative contributions of the ρ, ρ', and ρ'' resonances, as well as the mass and width of the ρ' meson. We assume that in a first approximation the widths of the ρ, ρ', and ρ'' resonances do not depend on the invariant mass of four pions. We use the extracted values of the mass and width of the ρ' to perform a full unbinned maximum likelihood fit of the $3\pi\pi^0$ final state.

To perform this fit, we use several phenomenological models. Besides the $\omega\pi$ channel, we allow for $a_1\pi$, $\sigma\rho$, $f_0\rho$, non-resonant $\rho\pi\pi$ and non-resonant $3\pi\pi^0$ channels, as well as for their various combinations, and fit for their relative contributions to the $3\pi\pi^0$ resonant structure.

With a better knowledge of the four pion subchannel structure, we then perform a fit to the $\tau \to \omega\pi\nu_\tau$ spectral function assuming a mass-dependent width for the three ρ resonances.

We do not use particle identification to separate pions from kaons and include components containing kaons (e.g., $K3\pi$) in the τ background. Generalization to charge conjugated reactions and final states is implied throughout this paper.

II. EXPERIMENT AND DATA SELECTION

We use data from the reaction $e^+e^- \to \tau^+\tau^-$ collected by the CLEO II experiment at the Cornell Electron Storage Ring (CESR) at or near the energy of the $\Upsilon(4S)$. The data correspond to a total integrated luminosity of $4.68\,\mathrm{fb}^{-1}$ and contain about 4.27 million $\tau^+\tau^-$ pairs.

CLEO II is a general-purpose solenoidal magnet detector [14]. The momenta of the charged particles are measured by a 67-layer drift chamber tracking system operating inside a 1.5 T superconducting solenoid. Photons and electrons are detected in a 7800-crystal CsI electromagnetic calorimeter. Muons are identified using proportional counters placed at various depths in the return iron of the magnet yoke.

The event selection is designed to use the kinematical properties and the low multiplicity of τ decays to separate them from events copiously produced in two-photon interactions, the process $e^+e^- \to q\bar{q}$, Bhabha scattering, and muon-pair production. We select events with four charged tracks in a 1-vs-3 topology by requiring that one of the tracks must be at least 90° away from all the others. When there is more than one combination satisfying these criteria, we minimize the acolinearity angle between the momentum of the single track and the total momentum of the 3-prong system to select the most back-to-back combination. The single track hemisphere is then used as a tag associated with a one-prong τ decay to $e\bar{\nu}_e\nu_\tau$, $\mu\bar{\nu}_\mu\nu_\tau$, $\pi\nu_\tau$, or $\rho\nu_\tau$. The other three tracks and at least two well identified photons, separated by more than 90° from the tag track, are used to reconstruct the hadronic part of the signal decay $\tau \to 3\pi\pi^0\nu_\tau \to 3\pi\gamma\gamma\nu_\tau$.

To ensure well modeled acceptance, momenta of the tracks from signal and tag hemispheres must exceed $0.025E_{bm}$ and $0.05E_{bm}$ respectively, where E_{bm} is the energy of the colliding electron or positron beam and lies between 5.26 and 5.29 GeV. To suppress decay channels with $K_s^0 \to \pi^+\pi^-$ decays, we require that the impact parameter of charged tracks with respect to the beam axis must be less than 5 mm. The momentum of a π^0 candidate is reconstructed from the energies and directions of two photons, constrained to the mass of the π^0. The two photon candidates must produce showers in the barrel part of the crystal calorimeter (i.e., $|\cos\theta_\gamma| < 0.71$, where θ_γ is the angle between the photon and e^+e^- beam axis) and be separated by more than 20° from the closest charged track. Energy deposition in the calorimeter is required to have a photon-like lateral profile and be greater than 75 MeV for the photon with the smaller energy and greater than 120 MeV for the photon with the higher energy. We consider only those two-photon combinations that are within 2.5 standard deviations from the nominal π^0 mass. To increase statistics for the rho tag, we also use showers in the tag hemisphere, detected both in the barrel and endcaps, with energy deposition greater than 30 MeV.

For electron identification, we require that the momentum of the track be greater than $0.5\,\mathrm{GeV}/c$ and that the energy deposited in the calorimeter be consistent with the momentum of the electron candidate measured by the drift chamber: $|(E/p - 1.0)| < 0.1$. We also require that the rate of energy loss due to ionization in the drift chamber must be no less than two standard deviations below the expected rate. A track is identified as a muon if it has correlated drift and muon chamber hits and traverses at least three absorption lengths of the material, when the momentum of the track is below $2\,\mathrm{GeV}/c$, and at least five absorption lengths, when the momentum of the track is above $2\,\mathrm{GeV}/c$. To minimize the probability of pion-lepton misidentification for both electron and muon tags, we do not allow additional showers in the calorimeter with energy deposition greater than 120 MeV that are unmatched to any of the charged tracks. A tag track is identified as a pion if it was not identified as a lepton and if the invariant mass of the tag hemisphere is less than $0.5\,\mathrm{GeV}/c^2$, where the invariant mass of the tag hemisphere is defined as the invariant mass of the tag track, assuming the pion mass, and all neutral showers in the tag hemisphere. A tag track is identified as a rho if it was not identified as a lepton, if the invariant mass of the two most energetic showers in the tag hemisphere is consistent with the π^0 mass within 2.5 standard deviations and, finally, if the effective mass of the tag track, assuming the pion mass, and of the π^0 candidate lies between 0.5 and $1.2\,\mathrm{GeV}/c^2$. To reduce combinatorial and hadronic background for the rho tag, we do not allow any showers with energy deposition greater than 120 (350) MeV in the tag hemisphere if the center of the

shower is more (less) than 30 cm from the tag track projection onto the calorimeter.

A typical event, in which the decay $\tau \to 3\pi\pi^0\nu_\tau$ is tagged by a one-prong τ decay, does not deposit any significant extra energy in the calorimeter, other than that associated with either the $\pi^0 \to \gamma\gamma$ decay or with interactions between charged hadrons and CsI crystals. In most cases, additional unmatched energy deposited in the calorimeter is a signature of various background events having one or more additional π^0's. To suppress these backgrounds, we use the value of the unmatched energy to veto such events. We reject events if there is at least one unmatched energy cluster in the calorimeter, which is not used for π^0 reconstruction, which is more (less) than 30 cm away from the closest projection of the charged track onto the calorimeter and which has energy deposition more than 75 (350) MeV.

Further background reduction is based on the fact that, in a τ decay, there is always at least one neutrino carrying away undetected energy and momentum. Thus, a typical τ event has a large missing transverse momentum, P_t, whereas a typical two photon event has a small missing transverse momentum and a small visible energy, E_{tot}. The transverse momentum and visible energy are measured using the four reconstructed charged tracks, assuming the pion masses for the three charged tracks in the signal hemisphere, and one π^0 (two π^0's for the rho tag). To remove two-photon background, we use the following selection criteria [15]: $P_t > 0.1(2E_{bm} - E_{tot})$, $P_t > 0.075E_{bm}$, and $E_{tot} > 0.6E_{bm}$. To reduce background produced by Dalitz decays $\pi^0 \to e^+e^-\gamma$ or by γ conversions in the detector, we reject any event that has a well identified electron among the three charged tracks in the signal hemisphere. To reduce combinatorial $q\bar{q}$ background, we impose a requirement on the undetected neutrino mass. The neutrino mass can be calculated as

$$M_\nu^2 = (P_\tau - P_q)^2 = M_\tau^2 + q^2 + 2|\vec{P}_\tau||\vec{P}_q|\cos\theta_{\tau q} - 2E_{bm}E_q. \tag{1}$$

Because we cannot measure $\cos\theta_{\tau q}$, we assume it to be 1 and require that the resulting maximum value of the square of the undetected neutrino mass be positive: $M^2_{\nu,max} > 0$. In Eq. (1) the value of M_τ is taken as $1.777\,\mathrm{GeV}/c^2$ [10], the momentum of the τ is expressed as $|\vec{P}_\tau| = \sqrt{E_{bm}^2 - M_\tau^2}$, the symbols q and E_q represent the invariant mass and energy of the four pion final state, and the energy of the τ is set equal to the beam energy E_{bm}.

The distribution of the $3\pi\pi^0$ effective mass, before the cut on the τ neutrino mass is applied, is plotted in Fig. 1. In the vicinity of the τ mass the production of $3\pi\pi^0$ events is strongly suppressed by phase space and the signal-to-background ratio becomes small. Hence, we accept only those events that have the effective mass of the $3\pi\pi^0$ final state lying in the range from 0.9 to $1.7\,\mathrm{GeV}/c^2$.

After all signal selection criteria are applied, we find 25 374 data events with an estimated background of 577 $\pm$17 events coming from $e^+e^- \to q\bar{q}$ production and 669 $\pm$230 events from other τ decays. The background estimates are based on Monte Carlo simulations. The latter background

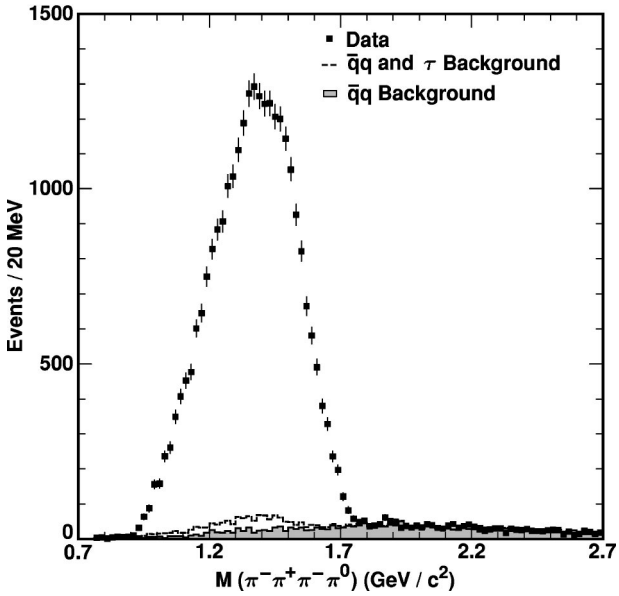

FIG. 1. The distribution of the invariant mass of $3\pi\pi^0$ is plotted for the data (dots), total background (dashed line) and $q\bar{q}$ background (hatched area), before the cut on the τ neutrino mass. Further analysis is limited to events between 0.9 and $1.7\,\mathrm{GeV}/c^2$.

source includes contributions from $\tau^- \to 2\pi^-\pi^+2\pi^0\nu_\tau$ and $\tau^- \to \pi^-\pi^0 K_s\nu_\tau \to 2\pi^-\pi^+\pi^0\nu_\tau$ decays whose yields in the final sample of signal events are estimated as 1.6% and 0.7%, respectively. The τ background also includes $K\pi\pi\pi^0$ and $KK\pi\pi^0$ components. Their contributions into the sample of signal events, calculated using the values [10] of $\mathcal{B}[\tau^- \to K^-\pi^+\pi^-\pi^0\nu_\tau(K_s^0 \text{ excluded})] = (0.024^{+0.043}_{-0.016})\%$ and $\mathcal{B}(\tau^- \to K^-K^+\pi^-\pi^0\nu_\tau) = (0.069 \pm 0.030)\%$ for the branching fractions, are 0.6% each. Background contamination from other τ decays is found to be negligible. The combined efficiency for all tags is estimated to be 6.75%. The measured branching fraction is $\mathcal{B}(\tau \to 3\pi\pi^0\nu_\tau) = (4.19 \pm 0.10)\%$, which does not include a conservatively estimated 5% systematic error associated with the data analysis. This is in good agreement with the Particle Data Group [10] value of $(4.35 \pm 0.10)\%$. Contamination due to 2γ physics is estimated to be negligible.

III. THE SPECTRAL FUNCTIONS IN $\tau \to 3\pi\pi^0\nu_\tau$ AND $\tau \to \omega\pi\nu_\tau$ DECAYS

The shape of the $3\pi\pi^0$ effective mass in τ decays is distorted by phase space and helicity factors. It is useful to examine the spectral function independent of such effects specific to τ decays.

The spectral function for $\tau \to 3\pi\pi^0\nu_\tau$ is defined [16] as

$$V^{3\pi\pi^0}(q) = \frac{d\Gamma_{4\pi\nu}(q)}{dq}\,\frac{16\pi^2 M_\tau^3}{G_F^2 V_{ud}^2}\,\frac{1}{q(M_\tau^2 - q^2)^2(M_\tau^2 + 2q^2)}, \tag{2}$$

where $q = M(3\pi\pi^0)$, $V_{ud} = 0.9740 \pm 0.0010$ is an element of the Cabibbo-Kobayashi-Maskawa (CKM) matrix [10] and G_F is the Fermi constant. The differential partial width can be represented as

$$\frac{d\Gamma_{4\pi\nu}(q)}{dq}=\frac{1}{N}\frac{dN(q)}{dq}\frac{G_F^2M_\tau^5}{192\pi^3}\frac{\mathcal{B}(\tau\to 3\pi\pi^0\nu_\tau)}{\mathcal{B}(\tau\to e\bar{\nu}_e\nu_\tau)}, \quad (3)$$

where a value of $\mathcal{B}(\tau\to e\bar{\nu}_e\nu_\tau)=0.1781\pm 0.0007$ [10] is taken. Thus, the spectral function is given by

$$V^{3\pi\pi^0}(q)=\frac{1}{N}\frac{dN(q)}{dq}\frac{1}{q(M_\tau^2-q^2)^2(M_\tau^2+2q^2)} \times\frac{\mathcal{B}(\tau\to 3\pi\pi^0\nu_\tau)}{\mathcal{B}(\tau\to e\bar{\nu}_e\nu_\tau)}\frac{M_\tau^8}{12\pi V_{ud}^2}. \quad (4)$$

To reduce uncertainty caused by the finite bin width, the factor $q(M_\tau^2-q^2)^2(M_\tau^2+2q^2)$ in the denominator is averaged over the bin width. To estimate systematic errors for the $V^{3\pi\pi^0}(q)$ spectral function, we take into account uncertainties in $\mathcal{B}(\tau\to e\bar{\nu}_e\nu_\tau)$ and V_{ud}.

In full analogy with $V^{3\pi\pi^0}(q)$, we can define a spectral function for the $\tau\to\omega\pi\nu_\tau$ decay. To extract the $\omega\pi$ component from the $3\pi\pi^0$ final state, we use a technique similar to the usual sideband subtraction. For each bin of $q=M(3\pi\pi^0)$, we select events in the ω signal region $[0.76\,\mathrm{GeV}/c^2<M(\pi^-\pi^+\pi^0)<0.81\,\mathrm{GeV}/c^2]$ and fit the combined sidebands $[0.83\,\mathrm{GeV}/c^2<M(\pi^-\pi^+\pi^0)<0.90\,\mathrm{GeV}/c^2]$ and $[0.60\,\mathrm{GeV}/c^2<M(\pi^-\pi^+\pi^0)<0.74\,\mathrm{GeV}/c^2]$ to a second order polynomial. The fit parameters are then used to estimate the background under the ω peak. To estimate the statistical uncertainty of the non-ω component in the signal region, we propagate errors using a full covariance matrix. In addition to the statistical error for each bin, there is an uncertainty due the sideband definition. To estimate the size of this error for each bin, we vary the sideband definition and change the order of the polynomial from 2 to 1. The distribution of the invariant mass $M(\pi^+\pi^-\pi^0)$ summed over all bins of $M(3\pi\pi^0)$ is shown in Fig. 2 together with a second order polynomial fit to the sidebands. This plot is presented for illustration only. The sideband subtraction procedure was performed separately for each bin of $M(3\pi\pi^0)$.

In Fig. 3 the shape of the $M(\omega\pi)$ distribution, which includes both ω signal component and combinatorial background, is shown with open squares. The non-$\omega\pi$ contribution is shown as a band for different sideband definitions, and its average value is shown with solid squares. For every bin, the error is calculated as a sum in quadrature of both statistical and systematic uncertainties.

Beginning with the distributions shown in Figs. 1 and 3, we subtract backgrounds, and apply efficiency corrections that were determined using a detailed Monte Carlo simulation of the τ decay process and the detector response. We then employ Eq. (4) to extract the spectral functions $V^{3\pi\pi^0}(q)$ and $V^{\omega\pi}(q)$, as well as the non-$\omega\pi$ contribution $V^{non-\omega\pi}(q)\equiv V^{3\pi\pi^0}(q)-V^{\omega\pi}(q)$. All three spectral components are shown in Fig. 4. The extracted $\omega\pi$ component is a product of the spectral function $V^{\omega\pi}(q)$ and the branching fraction $\mathcal{B}(\omega\to\pi^-\pi^+\pi^0)=0.888\pm 0.007$ [10] because we reconstruct ω in the three pion final state only.

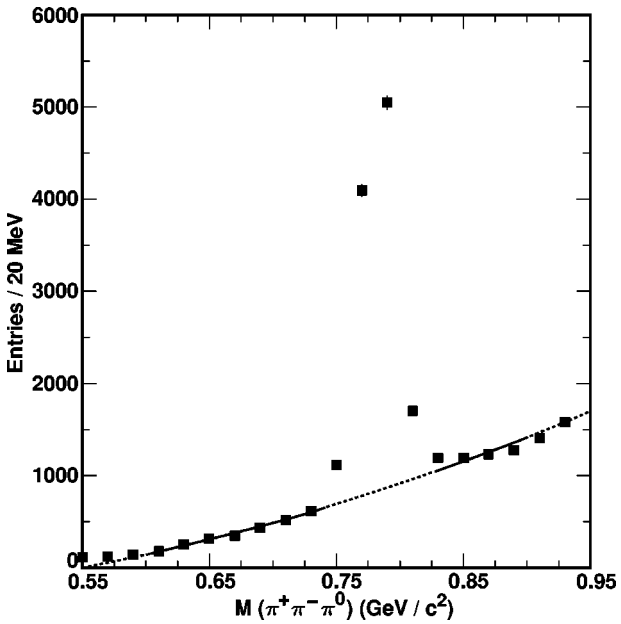

FIG. 2. Sideband fit to the invariant mass $M(\pi^+\pi^-\pi^0)$. The data are shown as solid squares, the second order polynomial fit is shown as a solid line, and the polynomial curve extrapolated into the regions excluded from the fit is shown as a dotted line.

IV. MODEL FITS TO THE $\tau\to\omega\pi\nu_\tau$ SPECTRAL FUNCTION

The spectral function of the $\omega\pi$ component can be expressed [16] in terms of the weak form factor $F(q)$ as

$$V^{\omega\pi}(q)=\frac{1}{12\pi}\left(\frac{p_\omega(q)}{q}\right)^3\left|\frac{g_{\rho\omega\pi}}{\gamma_\rho}F(q)\right|^2. \quad (5)$$

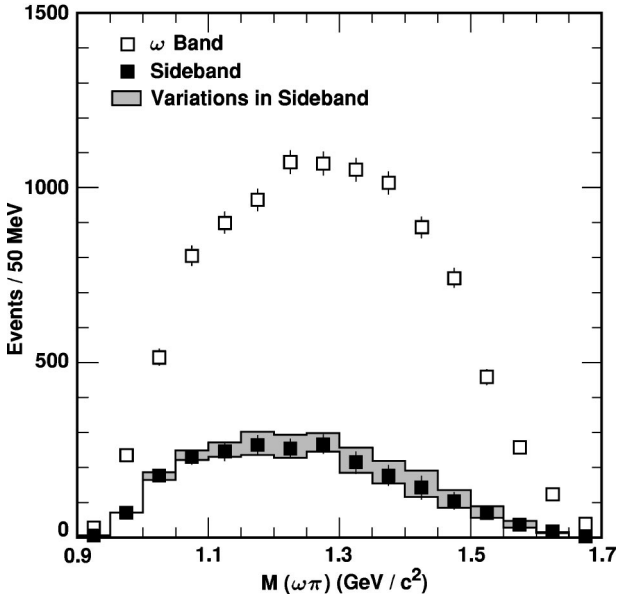

FIG. 3. Distributions of the $\omega\pi$ effective mass for events from the ω band (open squares) and the sidebands (solid squares). The ω band distribution includes combinatorial background as well. Variations in the shape of the combinatorial background due to variations in the sideband definition are shown as a band. The estimated average background shape, with errors, is shown with solid squares.

Here, $g_{\rho\omega\pi}$ is the $\rho\to\omega\pi$ strong decay coupling, γ_ρ is a measure of the weak coupling of the ρ resonance to the weak charged current, and

$$p_\omega(q)=\sqrt{\frac{(q^2-(M_\omega-M_\pi)^2)(q^2-(M_\omega+M_\pi)^2)}{4q^2}} \quad (6)$$

is the momentum of the ω in the $\omega\pi$ rest frame.

The choice of the form factor $F(q)$ is largely uncertain. In the region of $q\lesssim M_\tau$ the form factor $F(q)$ is expected to be dominated by low-energy vector resonances. In this analysis we use a form for $F(q)$ that allows contributions from the ρ resonance and its two radial excitations ρ' and ρ'':

$$F(q)=BW_\rho(q)+A_1\cdot BW_{\rho'}(q)+A_2\cdot BW_{\rho''}(q). \quad (7)$$

Here

$$BW_\rho(q)=\frac{M_\rho^2}{M_\rho^2-q^2-iq\Gamma_\rho} \quad (8)$$

is a relativistic Breit-Wigner amplitude normalized to unity at $q=0$, and

$$A_i=\frac{g_{\rho_i\omega\pi}}{g_{\rho\omega\pi}}\frac{\gamma_\rho}{\gamma_{\rho_i}} \quad (9)$$

are the ratios of the coupling constants for the different ρ resonances.

To model the Breit-Wigner shapes (8), we first approximate Γ_ρ, $\Gamma_{\rho'}$, and $\Gamma_{\rho''}$ by constants and do not include any momentum dependence. The parameters of the $\rho(770)$ resonance have been throroughly studied and are known with great precision [10]. In contrast, the parameters of the higher radial excitations ρ' and ρ'' are poorly known and can be used as fit variables. Unfortunately, events above $1.6\,\mathrm{GeV}/c^2$ are suppressed by phase space and provide little sensitivity for the heavy ρ'', the mass of which is expected to be around $1.7\,\mathrm{GeV}/c^2$. In this study we only fit for the mass and width of ρ' and keep widths and masses of ρ and ρ'' fixed at their central Particle Data Group (PDG) values [10]:

$$M_\rho=770\ \ \mathrm{MeV}/c^2;\quad \Gamma_\rho=151\ \ \mathrm{MeV}/c^2;$$

$$M_{\rho''}=1700\ \ \mathrm{MeV}/c^2;\quad \Gamma_{\rho''}=235\ \ \mathrm{MeV}/c^2. \quad (10)$$

The conserved vector current (CVC) hypothesis [16] predicts that the weak form factor and coupling constants are equal to the corresponding electromagnetic quantities. The weak coupling $W^\pm\to\rho^\pm\to\omega\pi^\pm$ in τ decays is expected to be the same as the electromagnetic coupling $\gamma^*\to\omega\pi^0$ in the reactions $e^+e^-\to\gamma^*(q_\gamma=\sqrt{s})\to\omega\pi^0$ and $\omega\to\gamma(q_\gamma=0)\pi^0$. All these couplings can be presented as $g_{\rho\omega\pi}/\gamma_\rho$, where

$$\gamma_\rho=\sqrt{\frac{4\pi^2\alpha^2M_\rho}{3\Gamma(\rho\to e^+e^-)}}. \quad (11)$$

Thus, one can use the vector dominance model [17] to cross-check the values of A_1 and A_2. In the VDM, the coupling constants are energy independent, and therefore the set of fitted coupling constants should reproduce the experimentally measured value of

$$\Gamma(\omega\to\pi^0\gamma)=\frac{1}{3}\alpha P_\gamma^3\cdot\left|\frac{g_{\rho\omega\pi}}{\gamma_\rho}[1+A_1+A_2]\right|^2$$
$$=(0.72\pm0.04)\ \ \mathrm{MeV}/c^2, \quad (12)$$

where P_γ is the photon momentum in the ω center-of-mass system.

To fit the data, we use the following spectral models:

Model 1: $F(q)\propto|BW_{\rho(770)}+A_1BW_{\rho'}+A_2BW_{\rho(1700)}|^2$.
Model 2: $F(q)\propto|BW_{\rho(770)}+A_1BW_{\rho'}|^2$.
Model 3: $F(q)\propto|BW_{\rho(770)}+A_2BW_{\rho(1700)}|^2$.
Model 4: $F(q)\propto|BW_{\rho(770)}|^2$.

The amplitudes A_1 and A_2 are assumed to be real. We use χ^2 minimization to fit various resonant models to the $\omega\pi$ spectral function shown in Fig. 5. To obtain this $\omega\pi$ spectral function, we divide the $\omega\pi$ spectral function shown in Fig. 4 by the branching fraction $\mathcal{B}(\omega\to\pi^-\pi^+\pi^0)=0.888\pm0.007$ because the four pion final state does not include contributions from other decays of the ω. We verified that the fit results are independent of the chosen initial values by repeating the minimization procedure with different sets of initial values.

The following parameters of the ρ' are obtained from fits to the data with models 1 and 2:

Model 1: $M_{\rho'}=(1.52\pm0.01)\ \ \mathrm{GeV}/c^2$;
$\Gamma_{\rho'}=(0.38\pm0.04)\ \ \mathrm{GeV}/c^2$;

Model 2: $M_{\rho'}=(1.53\pm0.01)\ \ \mathrm{GeV}/c^2$;
$\Gamma_{\rho'}=(0.43\pm0.03)\ \ \mathrm{GeV}/c^2$.

Using these results, we calculate weighted averages of the ρ' parameters: $M_{\rho'}=(1.523\pm0.010)\,\mathrm{GeV}/c^2$, $\Gamma_{\rho'}=(0.400\pm0.035)\,\mathrm{GeV}/c^2$.

Models 3 and 4 do not provide an acceptable description of the data. Fits to our data corresponding to various combinations of the ρ resonances are displayed in Fig. 5, and the results are summarized in Table I. We conclude that the presence of a ρ' contribution is necessary to achieve an acceptable description of the data. Model 2 is favored, but model 1 cannot be excluded.

V. INCLUSION OF MASS-DEPENDENT WIDTHS INTO THE FIT OF THE $\tau\to\omega\pi\nu_\tau$ SPECTRAL FUNCTION

We now perform a fit to the $\tau\to\omega\pi\nu_\tau$ spectrum assuming mass-dependent widths for the three ρ resonances. For this purpose, we use the results of Sec. VII E. We choose the model that includes contributions from $\omega\pi$, $\rho\pi\pi$, and nonresonant $3\pi\pi^0$ channels and use the extracted values of $R_{\rho^0\pi^-\pi^0}$, $R_{\rho^-\pi^-\pi^+}$, $R_{\rho^+\pi^-\pi^-}$, and $R_{\omega\pi}$ to perform a nu-

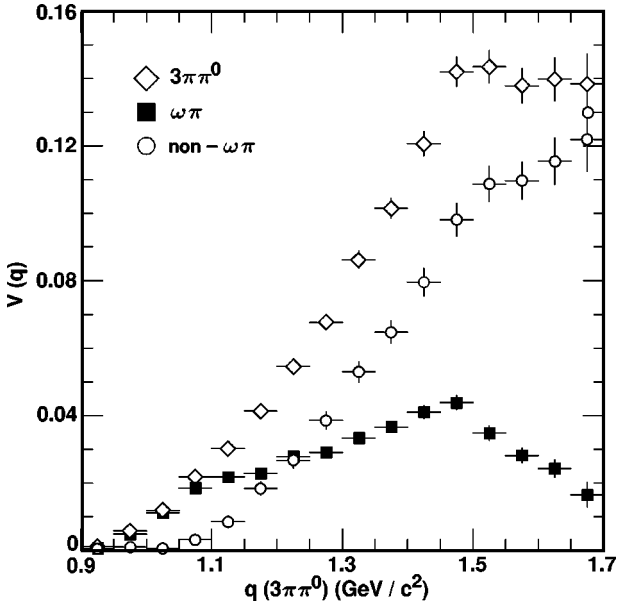

FIG. 4. Spectral functions calculated for $3\pi\pi^0$, $\omega\pi$ and non-$\omega\pi$ components. The spectral function $V^{\omega\pi}(q)$ is multiplied by $\mathcal{B}(\omega \to \pi^-\pi^+\pi^0) = 0.888 \pm 0.007$ because the ω is reconstructed in the three pion final state only.

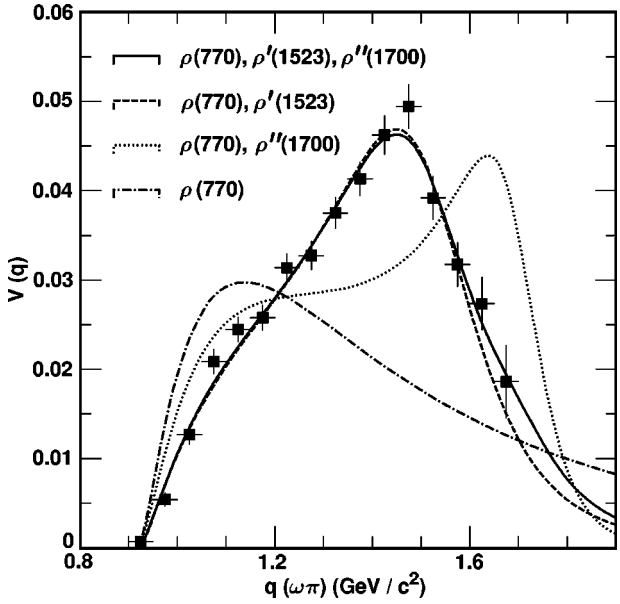

FIG. 5. Fits of the $\omega\pi$ spectral function with various models.

merical integration in momentum space in order to obtain a spectral decomposition of the $\tau \to 3\pi\pi^0\nu_\tau$ channel. The results of the integration are shown in Table II. To perform this integration, we use the value of the mass of the ρ' extracted from the fits to the $\omega\pi$ spectral function as described in the previous section.

With a better understanding of the $\omega\pi$ and $\rho\pi\pi$ spectral functions, we perform a fit to the $\tau \to \omega\pi\nu_\tau$ spectrum assuming mass-dependent widths for the three ρ resonances. Instead of constant-width Breit-Wigner shapes (8), we use mass-dependent total widths $\Gamma_i(q)$; $i = \rho, \rho', \rho''$. To simulate the mass-dependent widths, we follow the approach adopted in Ref. [6].

Since $\rho \to \pi\pi$ is the dominant ρ decay mode, we take into account only this channel for the calculation of $\Gamma_\rho(q)$:

$$\Gamma_\rho(q) = \Gamma_\rho \left(\frac{M_\rho}{q} \right)^2 \left(\frac{p_\pi(q)}{p_\pi(M_\rho)} \right)^3, \tag{13}$$

where $\Gamma_\rho = 151\,\mathrm{MeV}/c^2$ and $M_\rho = 770\,\mathrm{MeV}/c^2$ are the central width and mass of the ρ resonance fixed at their PDG values [10], q is the four pion invariant mass, $p_\pi(q) = \sqrt{q^2/4 - M_\pi^2}$ is the pion momentum in the ρ rest frame, and $p_\pi(M_\rho)$ is the same momentum evaluated at the pole mass of the ρ resonance.

For the total width of the ρ' resonance, we take into account only contributions from $\rho' \to \pi\pi$, $\rho' \to \omega\pi$, and $\rho' \to \rho\pi\pi$ modes:

$$\begin{aligned} \Gamma_{\rho'}(q) = \Gamma_{\rho'} \Bigg[& \mathcal{B}(\rho' \to \pi\pi) \left(\frac{M_{\rho'}}{q} \right)^2 \left(\frac{p_\pi(q)}{p_\pi(M_{\rho'})} \right)^3 \\ & + \mathcal{B}(\rho' \to \omega\pi) \left(\frac{M_{\rho'}}{q} \right)^2 \left(\frac{p_\omega(q)}{p_\omega(M_{\rho'})} \right)^3 \\ & + \mathcal{B}(\rho' \to \rho\pi\pi) \frac{F_{\rho\pi\pi}(q)}{F_{\rho\pi\pi}(M_{\rho'})} \Bigg], \end{aligned} \tag{14}$$

where $\Gamma_{\rho'}$ and $M_{\rho'}$ are the central width and mass of the ρ' resonance that are allowed to float in the fit, $\mathcal{B}(\rho' \to \pi\pi)$, $\mathcal{B}(\rho' \to \omega\pi)$, and $\mathcal{B}(\rho' \to \rho\pi\pi)$ are relative branching fractions normalized with their sum equal to one, and $p_\omega(q)$ is the momentum of the ω in the $\omega\pi$ rest frame (6). To extract

TABLE I. Fit results for various combinations of the ρ, ρ', ρ'' resonances to the $\tau \to \omega\pi\nu_\tau$ spectral function. Errors are statistical only and are strongly correlated. Errors on the total width $\Gamma(\omega \to \pi^0\gamma)$ are obtained by propagating the entire covariance matrix.

Model no.	$g_{\rho\omega\pi}$ $(\mathrm{MeV}^2/c)^{-1/2}$	A_1	A_2	χ^2/DOF	$\Gamma(\omega \to \pi^0\gamma)$ MeV
1	16.4 ± 0.6	-0.20 ± 0.04	-0.017 ± 0.016	16.1/11	0.87 ± 0.15
2	16.1 ± 0.6	-0.24 ± 0.02		16.6/12	0.78 ± 0.10
3	22.7 ± 0.2		-0.067 ± 0.017	342/14	2.3 ± 0.05
4	27.2 ± 0.2			940/15	3.9 ± 0.03
		$\Gamma(\omega)\mathcal{B}(\omega \to \pi^0\gamma)$			0.72 ± 0.04

TABLE II. Contributions to the spectral functions of the $\omega\pi$ and $\rho\pi\pi$ subchannels of $\tau\to 3\pi\pi^0\nu_\tau$.

	$\omega\pi$	$\rho\pi\pi$
non-resonant	7%	76%
$\rho(770)$	36%	0.2%
$\rho'(1520)$	12%	5%
constructive interference	47%	20%

the shape of $F_{\rho\pi\pi}(q)$, we generate a $\tau\to\rho\pi\pi\nu_\tau$ sample with overall phase-space and with $\omega\pi$ contributions eliminated. The form factor is defined as

$$F_{\rho\pi\pi}(q)=\frac{1}{(M_\tau^2+2q^2)(M_\tau^2-q^2)^2}\frac{1}{q}\frac{dN}{dq}, \qquad (15)$$

where dN/dq is the number of Monte Carlo events in a given bin of the invariant mass q. To obtain the shape parameters, we fit the form factor to a second order polynomial.

The choice of the relative branching fractions of ρ' is largely uncertain [10]. The ratio $\mathcal{B}(\rho'\to\rho\pi\pi)/\mathcal{B}(\rho'\to\omega\pi)$ can be extracted from our data. The relative contributions of the ρ' resonance into the $\omega\pi$ and $\rho\pi\pi$ spectral functions, shown in Table II, are 12% and 5%, respectively. Hence, the ratio of the branching fractions is estimated as

$$\frac{\mathcal{B}(\rho'\to\rho\pi\pi)}{\mathcal{B}(\rho'\to\omega\pi)}=\frac{0.05}{0.12}\frac{\mathcal{B}(\tau\to\rho\pi\pi\nu_\tau)}{\mathcal{B}(\tau\to\omega\pi\nu_\tau)},$$

where the ratio $\mathcal{B}(\tau\to\rho\pi\pi\nu_\tau)/\mathcal{B}(\tau\to\omega\pi\nu_\tau)$ is given by the results of our multidimensional fit described in Sec. VII E. We obtain $\mathcal{B}(\rho'\to\rho\pi\pi)/\mathcal{B}(\rho'\to\omega\pi)=0.61$ and vary the value of $\mathcal{B}(\rho'\to\pi\pi)$ in the fit to make sure that the outcome depends weakly on the input value. For the final result shown in Fig. 6, we use the constraint [10] $\mathcal{B}(\rho'\to\pi\pi)/\mathcal{B}(\rho'\to\omega\pi)\sim 0.32$.

To simulate the mass-dependent width of the ρ'', we account only for the $\rho''\to\rho\pi\pi$ decay because PDG [10] suggests that this is the dominant mode. The mass-dependent width of the ρ'' is calculated similarly to the $\rho'\to\rho\pi\pi$ contribution:

$$\Gamma_{\rho''}(q)=\Gamma_{\rho''}\frac{F_{\rho\pi\pi}(q)}{F_{\rho\pi\pi}(M_{\rho''})}, \qquad (16)$$

where $\Gamma_{\rho''}=235\,\mathrm{MeV}/c^2$ and $M_{\rho''}=1700\,\mathrm{MeV}/c^2$ are the central width and mass of the ρ'' resonance fixed at their PDG values [10], and $F_{\rho\pi\pi}(q)$ has the same shape as for $\Gamma_{\rho'}(q)$.

Assuming this model, we fit the $\tau\to\omega\pi\nu_\tau$ spectral function to the data. We make two fits: (1) the contribution of the ρ'' resonance is set to zero, and (2) the contribution of the ρ'' is allowed to float in the fit. In both situations the extracted mass of the ρ' is close to that of the ρ''. Hence, we cannot distinguish between the two resonances, and we assume that the shape of the spectral function is affected by the ρ' resonance only. The extracted mass and width of the ρ' are 1.63 ± 0.06 GeV and 0.65 ± 0.08 GeV, respectively.

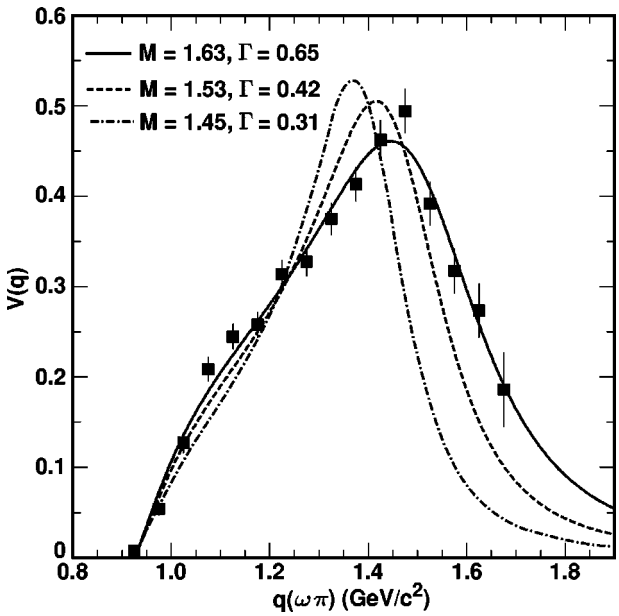

FIG. 6. Fits of the $\omega\pi$ spectral function with mass-dependent widths. The solid line represents the best fit, the dashed line represents the fit with the mass and width of the ρ' fixed at the values obtained from the mass-independent fit of Sec. IV, and the dashed-and-dotted line represents the fit with the mass and width of the ρ' fixed at their PDG values.

We also fit for the ρ' and ρ'' contributions fixing the masses and widths of the ρ' and ρ'' to their PDG values and to the values extracted from the fits with mass-independent widths as described in Sec. IV. The obtained fits do not reproduce the shape of the measured spectral function. All three fits are shown in Fig. 6.

Finally, we attempt to fit for the relative phases of the amplitudes A_1 and A_2, i.e., of the ρ' and ρ'' contributions, respectively. Our study shows that, varying the phases within $\pm\pi/4$, we do not introduce any significant changes in the shape of the spectral function. Hence, we can argue neither in favor of non-zero phases, nor in favor of phaseless models, and we set the phases to zero for simplicity.

We also fit the $\tau\to\omega\pi\nu_\tau$ spectral function, assuming another parametrization of the total width of the ρ' resonance. Now the $\rho'\to\rho\pi\pi$ contribution is replaced by that of $\rho'\to a_1\pi$ because Sec. VII E suggests that the four pion spectrum is dominated by the $\omega\pi$ and $a_1\pi$ channels. The last term in Eq. (14) is therefore replaced with $\mathcal{B}(\rho'\to a_1\pi)(M_{\rho'}/q)^2[p_{a_1}(q)/p_{a_1}(M_{\rho'})]$, where $\mathcal{B}(\rho'\to a_1\pi)$ is estimated using the results of Sec. VII E. The extracted values of the mass and width of the ρ' are similar to those quoted in this section, i.e., significantly larger than the values obtained with the mass-independent fit.

Because fits assuming mass-dependent widths rely heavily on the choice of the model for the width parameterization, we use the mass and width of the ρ' obtained in the fits with the mass-independent width (Sec. IV). The analysis described in this section has been included for completeness.

TABLE III. Expected shapes for different spin-parity assignments in the decay $\tau\to\omega\pi\nu_\tau$.

J^P	L	G	$F(\cos\chi)$
1^-	1	+1	$1-\cos^2\chi$
1^+	0	−1	1
1^+	2	−1	$1+3\cos^2\chi$
0^-	1	−1	$\cos^2\chi$

VI. SEARCH FOR SECOND CLASS CURRENTS IN THE DECAY $\tau\to\omega\pi\nu_\tau$

The decay $\tau\to\omega\pi\nu_\tau$ is expected to proceed through the hadronic vector current mediated by ρ, ρ', ρ'' and higher excitations. If, however, G parity conservation is broken due to second class currents [13], the decay can proceed through a hadronic axial-vector current mediated, e.g., by the $b_1(1235)$ resonance. The difference in spin-parity assignments for each of these states is reflected in different polarizations of the ω spin and hence in different expected angular distributions of $\cos\chi$. The angle χ is defined as the angle between the normal to the ω decay plane and the direction of the fourth pion measured in the ω rest frame. The expected forms [18] of the $\cos\chi$ distribution are listed in Table III for different orbital angular momenta L of the $\omega\pi$ system.

We form the distribution of $\cos\chi$ for the $\tau\to\omega\pi\nu_\tau$ events in our data. To eliminate combinatorial and non-ω background, we perform a sideband subtraction for every bin, in the same way as described in Sec. III. Using Monte Carlo estimates, we subtract small ω contributions from other τ decays and $q\bar{q}$ background events, correct for efficiency, and fit the resulting distribution, shown in Fig. 7, with the following function:

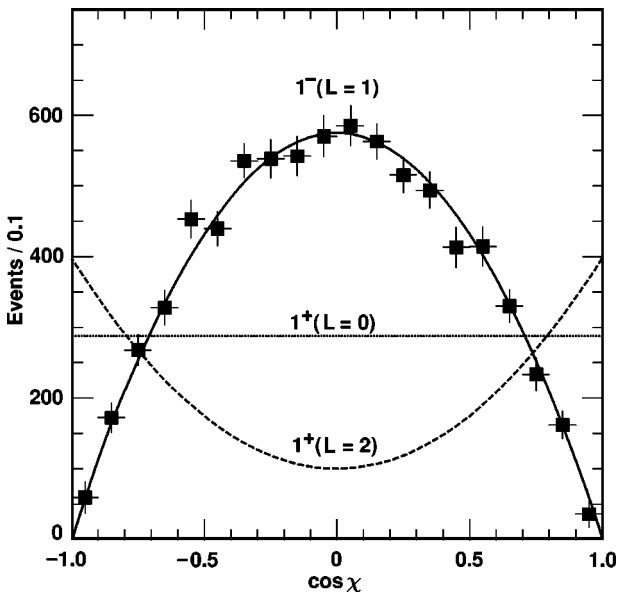

FIG. 7. The distribution of $\cos\chi$ for the $\tau\to\omega\pi\nu_\tau$ component after background subtraction and efficiency correction is shown with filled squares. The solid line represents the fit to the vector current model $J^P_L=1^-_1$, the dashed line shows the expected shape for $J^P_L=1^+_2$, and the dotted line shows the $J^P_L=1^+_0$ model.

$$F=(1-\epsilon)\cdot F^1+\epsilon\cdot F^2. \tag{17}$$

Here, $F^1(\cos\chi)=1-\cos^2\chi$ is the shape of the dominant vector contribution and $F^2(\cos\chi)=1$ represents the shape which gives the most conservative estimate of the non-standard contribution to the $\tau\to\omega\pi\nu_\tau$ decay. The value of ϵ obtained from the fit is consistent with zero within errors: $\epsilon=(0.08\pm 2.00)\times 10^{-2}$. After integration, it can be translated into an upper limit on the ratio $N^{\omega\pi}$ (non-vector current)/$N^{\omega\pi}$ (vector current)$<5.4\%$ at 90% CL and $<6.4\%$ at 95% CL, where $N^{\omega\pi}$ represents the number of events generated through the corresponding current. An analogous study [4] by ALEPH gave $N^{\omega\pi}$ (non-vector current)/$N^{\omega\pi}$ (vector current) $<8.6\%$ at 95% CL. The solid line in Fig. 7 illustrates the agreement of the $(1-\cos^2\chi)$ description and the data.

VII. FULL UNBINNED LIKELIHOOD FIT TO THE $\tau\to 3\pi\pi^0\nu_\tau$ RESONANT STRUCTURE

A general method of obtaining a resonant decomposition of a hadronic final state is a partial wave analysis of data via an unbinned maximum likelihood fit. For any data set with limited statistics, the analysis is model-dependent because there is a necessary choice of amplitudes to be considered. In this study, we consider four models with contributions from $\omega\pi$, $a_1\pi$, $\sigma\rho$, $f_0\rho$, $\rho\pi\pi$, and non-resonant $3\pi\pi^0$ channels.

Results depend on the model chosen for the hadronic current parametrization. A general description and some details of the formalism are given below. The amplitude description is given in the Appendix.

A. Definition of the fit function

The differential width of the τ decay into the $3\pi\pi^0$ final state is described by a factorizable sequence of decays: $\tau\to h+\nu_\tau$ followed by $h\to 4\pi$, and can be expressed as

$$d\Gamma(\tau\to 3\pi\pi^0\nu_\tau)=\frac{1}{2M_\tau}|\mathcal{M}|^2 d\mathrm{LIPS}(\tau\to\nu_\tau h)\times d\mathrm{LIPS}(h\to 3\pi\pi^0), \tag{18}$$

where

$$|\mathcal{M}|^2=\frac{G_F^2}{2}V_{ud}^2 L^{\mu\nu}H_{\mu\nu} \tag{19}$$

is the square of the corresponding matrix element, dLIPS is an element of the phase space volume, and $L^{\mu\nu}$ and $H_{\mu\nu}$ are lepton and hadronic tensors, respectively.

The lepton tensor $L^{\mu\nu}$ cannot be calculated without information on the neutrino direction. To resolve this problem, we use a general form of the matrix element [7] which is explicitly averaged over the neutrino direction. In this approach the averaged matrix element is expressed as a sum of 16 terms:

$$\overline{L^{\mu\nu}H_{\mu\nu}}=2(M_\tau^2-q^2)\sum_{i=1}^{16}\overline{L_i}W_i, \tag{20}$$

where the weights W_i can be calculated from components of the complex hadronic current J_μ, and $\overline{L_i}$ are kinematic parameters which depend only on the four-momenta of the four pions in the $3\pi\pi^0$ final state.

To calculate J_μ, we use the KORALB Monte Carlo program with the TAUOLA decay package [19]. The reconstructed four-momenta of the $2\pi^-\pi^+\pi^0$ system are boosted into the rest frame of the hadronic system which is denoted by the superscript ''cm.'' They are then projected onto the following coordinate system: the x-axis is along the direction of $(\vec{P}^{cm}_{\pi^+}+\vec{P}^{cm}_{\pi^0})$, the z-axis is perpendicular to the plane defined by the vectors $\vec{P}^{cm}_{\pi^-_1}$ and $\vec{P}^{cm}_{\pi^-_2}$, and the y-axis is perpendicular to the $x-z$ plane. We exclude a small region $\cos\psi > -0.97$, where some projections become poorly defined. Here, ψ is the angle [6] between the direction of the laboratory and the τ, as seen from the hadronic rest frame.

To check whether the calculation of the $\overline{L^{\mu\nu}H_{\mu\nu}}$ expression is correct, we choose a parametrization of the hadronic current with form factors and coupling constants that provide a good description of the data. We generate a large sample of $\tau\to 3\pi\pi^0\nu_\tau$ events according to the phase space and for each event we calculate the corresponding averaged weight $\overline{L^{\mu\nu}H_{\mu\nu}}$. As a cross check, we use the same parametrization of the hadronic current to generate another sample of unit weight events using the standard full TAUOLA simulation. The full $\tau\to 3\pi\pi^0\nu_\tau$ simulation invokes explicit generation of neutrino momenta and subsequent calculation of the precise matrix element $L^{\mu\nu}H_{\mu\nu}$. In the limit of large statistics, both methods should give the same results. The shapes of submass and total hadronic energy distributions generated with both methods agree, though the distributions obtained with the averaged matrix element reveal a higher level of fluctuations. This is due to the fact that the averaging over the neutrino direction introduces an additional smearing which increases errors.

B. Likelihood function

The matrix element averaged over the neutrino direction can be used as a probability density function (PDF) to fit the data of the $\tau\to 3\pi\pi^0\nu_\tau$ decays. The fitting technique is a straightforward extension of that used to fit three-body Dalitz plots.

We take advantage of the following convenient notation [15]. The matrix element $\mathcal{M}(\vec{\alpha},\vec{\beta}|\vec{\theta})$ is described by a model with a parameter vector $\vec{\theta}$ which consists of resonant amplitudes and phases. The matrix element is a function of observable variables $\vec{\alpha}$ (e.g., hadronic four-momenta) and non-observable variables $\vec{\beta}$ (e.g., neutrino four-momentum). The matrix element has to be integrated over the non-observable variables

$$f_S(\vec{\alpha}|\vec{\theta})=\int |\mathcal{M}(\vec{\alpha},\vec{\beta}|\vec{\theta})|^2 d\vec{\beta}, \tag{21}$$

where $f_S(\vec{\alpha}|\vec{\theta})$ is the probability to observe a final state with the parameter vector $\vec{\alpha}$, given the model parameters $\vec{\theta}$. To compare f_S directly with the data distribution, f_S must be multiplied by the phase space function $\phi(\vec{\alpha})$ and by the detector acceptance $\eta(\vec{\alpha})$:

$$f_S^{exp}(\vec{\alpha}|\vec{\theta})=\eta(\vec{\alpha})\phi(\vec{\alpha})f_S(\vec{\alpha}|\vec{\theta}). \tag{22}$$

To enforce the proper normalization of the signal PDF, we divide it by the integral taken over the observable space $\vec{\alpha}$:

$$F_S(\vec{\alpha}|\vec{\theta})=\frac{f_S(\vec{\alpha}|\vec{\theta})}{N(\vec{\theta})}=\frac{f_S(\vec{\alpha}|\vec{\theta})}{\int \eta(\vec{\alpha})\phi(\vec{\alpha})f_S(\vec{\alpha}|\vec{\theta})d\vec{\alpha}}. \tag{23}$$

Since the parameters of the PDF are varied in the fit, the normalization of the matrix element is no longer constant and must be recalculated on each step of the fit. Due to the presence of background, we must also include a corresponding background PDF $F_B(\vec{\alpha})$, and define the total PDF as:

$$F^{total}(\vec{\alpha}|\vec{\theta})=\frac{R_{S/B}F_S(\vec{\alpha}|\vec{\theta})+F_B(\vec{\alpha})}{R_{S/B}+1}, \tag{24}$$

where $R_{S/B}$ is a signal-to-background ratio. As usually, the likelihood function is defined by exchanging the argument and the parameter in the expression for $F^{total}(\vec{\alpha}|\vec{\theta})$. The likelihood function for selected events is then given by

$$\mathcal{L}(\vec{\theta})=\prod_{events} F^{total}=\prod_{events}\frac{R_{S/B}F_S+F_B}{R_{S/B}+1}\eta(\vec{\alpha})\phi(\vec{\alpha}). \tag{25}$$

To find the maximum of the likelihood, we minimize $-2\log\mathcal{L}$, where

$$\log\mathcal{L}(\vec{\theta})=\sum_{events}\log\frac{R_{S/B}F_S+F_B}{R_{S/B}+1}+\sum_{events}\log(\eta(\vec{\alpha})\phi(\vec{\alpha})). \tag{26}$$

The term $\Sigma\log[\eta(\vec{\alpha})\phi(\vec{\alpha})]$ is constant for the purpose of minimizing $\log\mathcal{L}(\vec{\theta})$ and is therefore neglected. Thus, we never need to evaluate explicitly $\eta(\vec{\alpha})$ and $\phi(\vec{\alpha})$: the amplitude normalization $N(\vec{\theta})$ obtained by Monte Carlo techniques takes them into account automatically. When parameter terms can be factored out, the computation of the normalization $N(\vec{\theta})$ can be speeded up:

$$\begin{aligned} N(\vec{\theta}) &= \int \eta(\vec{\alpha})\phi(\vec{\alpha})f_S(\vec{\theta}|\vec{\alpha})d\vec{\alpha} \\ &= \int \eta(\vec{\alpha})\phi(\vec{\alpha})\left[\sum_j C_j(\vec{\theta})f_j(\vec{\alpha})\right]d\vec{\alpha} \\ &= \sum_j C_j(\vec{\theta})\int \eta(\vec{\alpha})\phi(\vec{\alpha})f_j(\vec{\alpha})d\vec{\alpha}, \end{aligned} \tag{27}$$

where the index j runs over all possible combinations of the fit parameters $\vec{\theta}$. During the fit, the integrals in the above

expression are calculated only once and then multiplied by the coefficients C_j which depend on the parameters $\vec{\theta}$ only.

C. Signal PDF

As shown in Sec. VII B, all constant factors and functions of observable variables $\vec{\alpha}$ that multiply the signal PDF (21) do not change the position of a maximum of the likelihood function (25) in the parameter space $\vec{\theta}$. Neglecting such contributions, the signal PDF (21) can be expressed as

$$f_S=\overline{L^{\mu\nu}H_{\mu\nu}}=\sum_1^{16}\overline{L}_i W_i, \tag{28}$$

where the weigths W_i are calculated [7] from components of the hadronic current J_μ. The hadronic current for the decay $\tau^-\to 3\pi\pi^0\nu_\tau$ is parametrized as follows:

$$J^\mu=\alpha_\omega f_\omega^\mu F_\omega(q)+\sum_k \alpha_k f_k^\mu F_k(q), \tag{29}$$

where q is the hadronic invariant mass. The spectral functions (amplitude form factors) are defined as sums of the corresponding Breit-Wigner amplitudes

$$F_k(q)=\beta_k^0+\beta_k BW_\rho(q)+\beta_k' BW_{\rho'}(q)+\beta_k'' BW_{\rho''}(q). \tag{30}$$

The coefficients f_k^μ are functions of four-momenta of the four pions, the coefficients α_k are complex amplitudes, the coefficients β_k, β_k', and β_k'' are complex amplitudes of the kth spectral function component, and the sum in Eq. (29) is taken over all non-ω contributions, as described in Sec. VII E below. For practical purposes, the amplitude of one of the α_k is set to a non-zero constant and the phase of one of the α_k is set to zero; the corresponding rescaling factors are then included into the other amplitudes, while the overall normalization of the signal PDF is set to unity. The explicit form of the form factor f_ω^μ, based on Refs. [19–22] and shown in the Appendix, employs correct ω helicity factors and proper symmetrization.

From the fit, we determine the amplitudes α_k for the decay $\tau\to 3\pi\pi^0\nu_\tau$. We integrate these amplitudes over a large sample of $\tau\to 3\pi\pi^0\nu_\tau$ events to translate them into relative branching fractions.

D. Background PDF

The total background in the selected data sample is estimated to be 4.9%. Because it is small, we do not calculate a PDF for each individual component separately. Instead, we use a simpler, empirical approach: we reweight the $3\pi\pi^0$ phase space to create an effective matrix element describing the shape of the sum of the τ and $q\bar{q}$ backgrounds that was determined using detailed Monte Carlo simulations. We use a purely empirical form of this effective matrix element:

$$F_B=[M_\tau^2-M(3\pi\pi^0)^2]\left[1+\frac{0.8}{(M(\pi^0\pi_1^-)^2-M_\rho^2)^2+\Gamma_\rho^4}+\frac{0.8}{(M(\pi^0\pi_2^-)^2-M_\rho^2)^2+\Gamma_\rho^4}+\frac{0.011}{(M(\pi^0\pi^+\pi_1^-)^2-M_\omega^2)^2+\Gamma_\omega^4}\right.$$
$$\left.+\frac{0.011}{(M(\pi^0\pi^+\pi_2^-)^2-M_\omega^2)^2+\Gamma_\omega^4}+\frac{0.005}{(M(\pi_1^-\pi^+)^2-M_{K_s}^2)^2+\Gamma_{K_s}^4}+\frac{0.005}{(M(\pi_2^-\pi^+)^2-M_{K_s}^2)^2+\Gamma_{K_s}^4}\right]. \tag{31}$$

The choice of the parametrization is largely *ad hoc*, the coefficients are tuned to describe the background distributions in six mass projections, as shown in Fig. 8. These distributions are obtained from Monte Carlo simulations of τ backgrounds and an appropriately scaled contribution from $e^+e^-\to q\bar{q}$ continuum events.

E. Fits to various models

We use 4 models to parametrize the hadronic current. The models account for the following contributions:

Model 1: $\omega\pi$, $\rho\pi\pi$ and non-resonant $3\pi\pi^0$;
Model 2: $\omega\pi$ and $a_1\pi$;
Model 3: $\omega\pi$, $a_1\pi$, $\sigma\rho$, and $f_0(980)\rho$;
Model 4: $\omega\pi$, $a_1\pi$, and $\rho\pi\pi$.

Hadronic current expressions for each model are given in the Appendix. For the $\rho\pi\pi$ contribution, the spectral functions for the $\rho^-\pi^+\pi^-$, $\rho^0\pi^0\pi^-$, and $\rho^+\pi^-\pi^-$ components are assumed to be identical, and the corresponding form factors f_i^μ are parametrized in the same way as in the TAUOLA package [19]. We use the PDG [10] value for the mass of the a_1 resonance ($M_{a_1}=1230\,\mathrm{MeV}/c^2$) and adopt the prescription of Ref. [5] to use the higher end of the width interval recommended by PDG: $\Gamma_{a_1}=600\,\mathrm{MeV}/c^2$. For the mass and width of σ, i.e., $f_0(400-1200)$ in PDG's notation, we assume values [23] of $M_\sigma=860\,\mathrm{MeV}/c^2$ and $\Gamma_\sigma=880\,\mathrm{MeV}/c^2$. We use PDG values for the mass and width of the $f_0(980)$ of $M_{f_0}=980\,\mathrm{MeV}/c^2$ and $\Gamma_{f_0}=70\,\mathrm{MeV}/c^2$. To obtain the relative contributions of the $\tau\to 3\pi\pi^0\nu_\tau$ decay components, the fit parameters are integrated over 300 000 of $3\pi\pi^0$ phase space events and renormalized. Fit errors are propagated in accordance with this procedure. We use the following definition: $R_i=\mathcal{B}_i/\mathcal{B}(\tau^-\to 2\pi^-\pi^+\pi^0\nu_\tau)$, where $\mathcal{B}_i$ is a branching fraction for the corresponding channel, e.g., $R_{a_1\pi}=\mathcal{B}(\tau^-\to(a_1\pi)^-\nu_\tau)/\mathcal{B}(\tau^-\to 2\pi^-\pi^+\pi^0\nu_\tau)$. Statistical errors on the relative fractions R_i are obtained from the maximum likelihood fits assuming one standard deviation.

TABLE IV. Fit results for various models. R_i is defined as $R_i = \mathcal{B}_i / \mathcal{B}(\tau^- \to 2\pi^-\pi^+\pi^0\nu_\tau)$, e.g., $R_{a_1\pi} = \mathcal{B}(\tau^- \to (a_1\pi)^-\nu_\tau)/\mathcal{B}(\tau^- \to 2\pi^-\pi^+\pi^0\nu_\tau)$. The first error is statistical, and the second error is systematic.

Model	Integrated amplitudes	Sum of amplitudes	Goodness-of-fit
	$R_{\rho^0\pi^-\pi^0} = 0.11 \pm 0.01 \pm 0.02$		
	$R_{\rho^-\pi^-\pi^+} = 0.19 \pm 0.02 \pm 0.04$		
Model 1	$R_{\rho^+\pi^-\pi^-} = 0.23 \pm 0.02 \pm 0.04$	$0.93 \pm 0.04 \pm 0.08$	15%
	$R_{\omega\pi} = 0.40 \pm 0.02 \pm 0.05$		
	$R_{3\pi\pi^0} < 0.06$ at 95% CL		
Model 2	$R_{\omega\pi} = 0.38 \pm 0.02 \pm 0.02$	$0.81 \pm 0.03 \pm 0.03$	$<5\%$
	$R_{a_1\pi} = 0.43 \pm 0.02 \pm 0.02$		
	$R_{\omega\pi} = 0.38 \pm 0.02 \pm 0.01$		
Model 3	$R_{a_1\pi} = 0.49 \pm 0.02 \pm 0.02$	$0.89 \pm 0.03 \pm 0.03$	20%
	$R_{\sigma\rho} = 0.01 \pm 0.02 \pm 0.01$		
	$R_{f_0\rho} = 0.01 \pm 0.01 \pm 0.01$		
	$R_{\omega\pi} = 0.39 \pm 0.02 \pm 0.01$		
	$R_{a_1\pi} = 0.50 \pm 0.03 \pm 0.01$		
Model 4	$R_{\rho^0\pi^-\pi^0} = 0.01 \pm 0.01 \pm 0.01$	$0.93 \pm 0.04 \pm 0.02$	20%
	$R_{\rho^-\pi^-\pi^+} = 0.02 \pm 0.03 \pm 0.01$		
	$R_{\rho^+\pi^-\pi^-} = 0.01 \pm 0.01 \pm 0.01$		

To simulate the form factors $BW_{\rho'}$, BW_{a_1}, and BW_σ, we use both fits with mass-dependent and mass-independent widths. The observed variation in the amplitude values is small and has been included in the total systematic error. We fix the values of the mass and central width of ρ' in the fit; if these parameters are allowed to vary, the fit becomes unstable.

To estimate the goodness-of-fit for each model, we generate 40 Monte Carlo samples with the matrix element averaged over the neutrino direction. Each sample is generated with parameters obtained in the fit to the data and the number of events in each sample is approximately equal to that observed in the data. The goodness-of-fit is estimated as a fraction of samples where $-2\log\mathcal{L}$ exceeds that in the data.

Integrated amplitudes with statistical and systematic errors, as well as the confidence levels of the fits for the four chosen models, are listed in Table IV. The calculation of the systematic errors is explained in the following section. Projections of the fits on various mass combinations are shown in Figs. 9–11.

Models 3 and 4 provide the best description of the data. Both these models are dominated by $\omega\pi$ and $a_1\pi$ with small additional contributions of the $\sigma\rho$, $f_0\rho$, or non-resonant

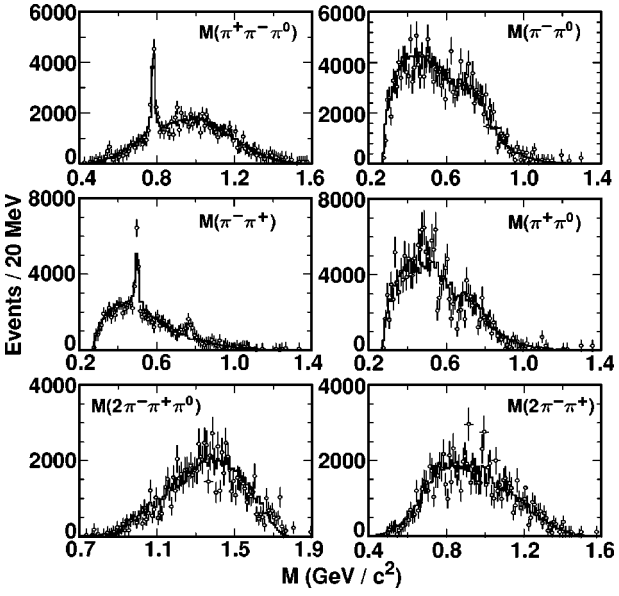

FIG. 8. Background parametrization plotted for different submass projections. The predictions from Monte Carlo simulations are shown with open dots. The background parametrization is shown as a histogram.

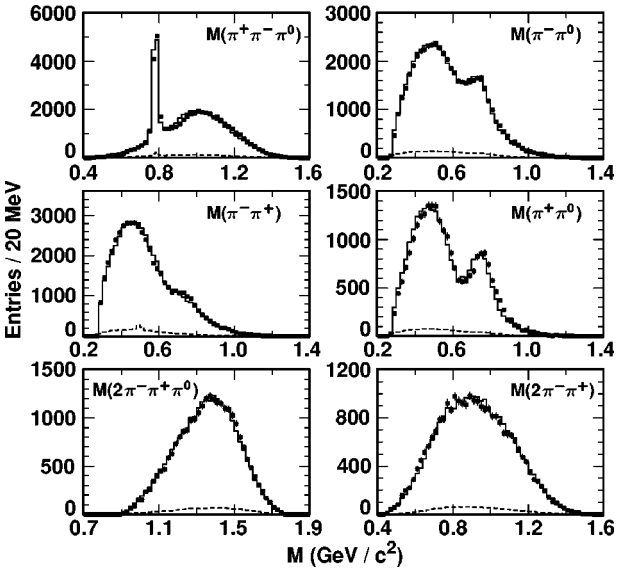

FIG. 9. Comparison between fits and data distributions for model 1. Solid squares represent the data, solid line represents the nominal fit, and the dashed line represents the parametrized background.

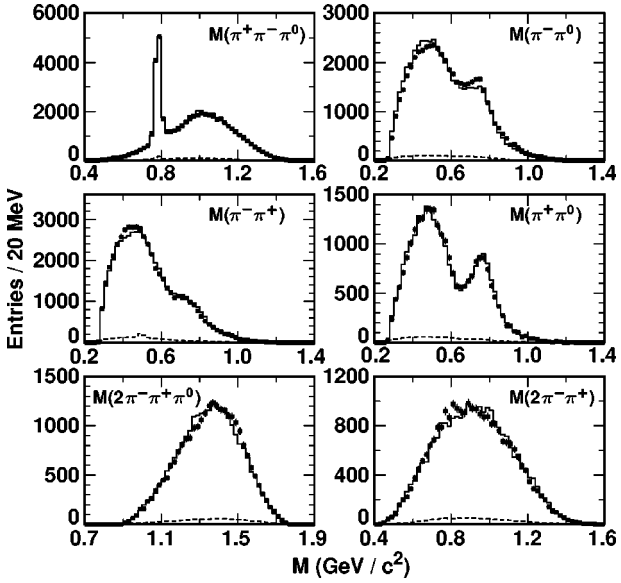

FIG. 10. Comparison between fits and data distributions for model 2. Solid squares represent the data, solid line represents the nominal fit, and the dashed line represents the parametrized background.

$\rho\pi\pi$ channels. Submass projections for models 3 and 4 are almost identical, and we show only those for model 3.

The presence of a non-resonant $3\pi\pi^0$ contribution does not improve the goodness-of-fit in model 1, and we set an upper limit on the non-resonant $3\pi\pi^0$ contribution, as shown in Table IV. We also ignore the non-resonant $3\pi\pi^0$ component in the three other models.

F. Systematic errors

To estimate systematic biases and errors for every model, we generate 40 Monte Carlo samples with amplitudes obtained from the fit to the data and then fit them to the chosen parametrization of the hadronic current. Each sample is mixed with simulated background events in the proportion expected from the data. We integrate the results of each simulation to estimate necessary corrections and systematic errors for each of the amplitudes. The biases of the reconstructed amplitude values are shown in Table V. The errors are determined as root mean squares of the parameter fluctutations.

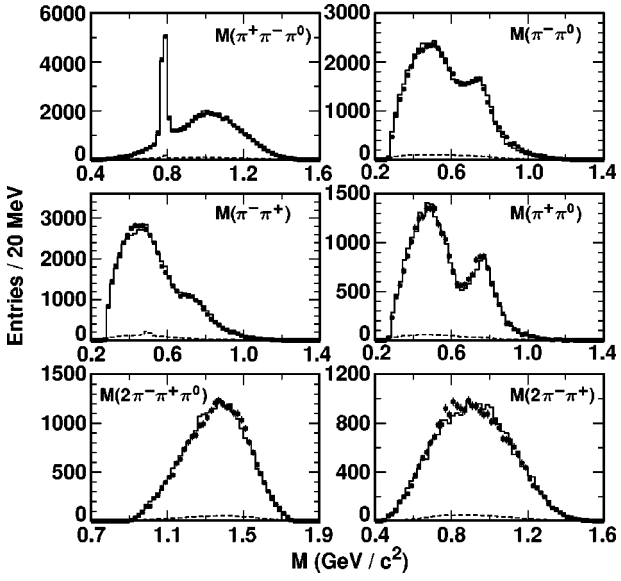

FIG. 11. Comparison between fits and data distributions for model 3. Solid squares represent the data, solid line represents the nominal fit, and the dashed line represents the parametrized background.

TABLE V. Systematic biases for the integrated contributions of different channels into the $\tau^- \to 2\pi^-\pi^+\pi^0\nu_\tau$ final state. Systematic bias is defined as $\delta_i = (R_i^{reconstructed} - R_i^{generated})/R_i^{generated}$.

Model	Systematic bias δ_i
Model 1	$\delta_{\rho^0\pi^-\pi^0} = (+4.0 \pm 3.8)\%$
	$\delta_{\rho^-\pi^-\pi^+} = (-7.6 \pm 3.8)\%$
	$\delta_{\rho^+\pi^-\pi^-} = (+2.3 \pm 2.6)\%$
	$\delta_{\omega\pi} = (+2.5 \pm 2.6)\%$
	$\delta_{3\pi\pi^0} = (+1.2 \pm 9.0)\%$
Model 2	$\delta_{\omega\pi} = (+1.0 \pm 2.5)\%$
	$\delta_{a_1\pi} = (-2.0 \pm 2.5)\%$
Model 3	$\delta_{\omega\pi} = (+1.0 \pm 2.5)\%$
	$\delta_{a_1\pi} = (-2.0 \pm 2.6)\%$
	$\delta_{\sigma\rho} = (0.0 \pm 14.0)\%$
	$\delta_{f_0\rho} = (+1.0 \pm 16.0)\%$
Model 4	$\delta_{\omega\pi} = (+1.0 \pm 2.5)\%$
	$\delta_{a_1\pi} = (-2.0 \pm 2.5)\%$
	$\delta_{\rho^0\pi^-\pi^0} = (1.0 \pm 23.0)\%$
	$\delta_{\rho^-\pi^-\pi^+} = (-0.0 \pm 15.0)\%$
	$\delta_{\rho^+\pi^-\pi^-} = (-2.5 \pm 33.0)\%$

The total systematic error also includes uncertainty due to the choice of the parameters of the ρ'. We use PDG [10] values for the masses and widths of the ρ and ρ'' mesons and vary the ρ' parameters within the errors obtained in the fit described in Sec. IV. We also switch to a smaller mass of the ρ' [12]: $M_{\rho'} = 1370\ \mathrm{MeV}/c^2$. The results appear to have little sensitivity to the choice of the parameters for the ρ'.

All contributions to the systematic error are added in quadrature. The systematic biases for the components of the hadronic current are shown in Table V.

G. Comparison with similar analyses

A recent analysis by the ALEPH Collaboration [4] assumes $\omega\pi$ and non-resonant $\rho\pi\pi$ contributions and uses a simplified fit to the submass projections without assigning systematic errors. This analysis by ALEPH gives the following amplitudes: $R_{\rho^0\pi^-\pi^0} = 0.11 \pm 0.01$, $R_{\rho^-\pi^-\pi^+} = 0.20 \pm 0.01$, $R_{\rho^+\pi^-\pi^-} = 0.22 \pm 0.01$, and $R_{\omega\pi} = 0.40 \pm 0.06 \pm 0.05$; these values are consistent with our results based on model 1. Predictions from the chiral perturbation theory [22] for the same model give: $R_{\rho^-\pi^-\pi^+} = 0$, $R_{\rho^+\pi^-\pi^-}/R_{\rho^0\pi^-\pi^0} = 2$. Our results are in disagrement with those obtained by ARGUS [3]: $R_{\rho^0\pi^-\pi^0} = 0.30 \pm 0.04 \pm 0.02$, $R_{\rho^-\pi^-\pi^+} = 0.26 \pm 0.05 \pm 0.01$, $R_{\rho^+\pi^-\pi^-} = 0.10 \pm 0.03 \pm 0.004$, and $R_{\omega\pi} = 0.33 \pm 0.04 \pm 0.02$.

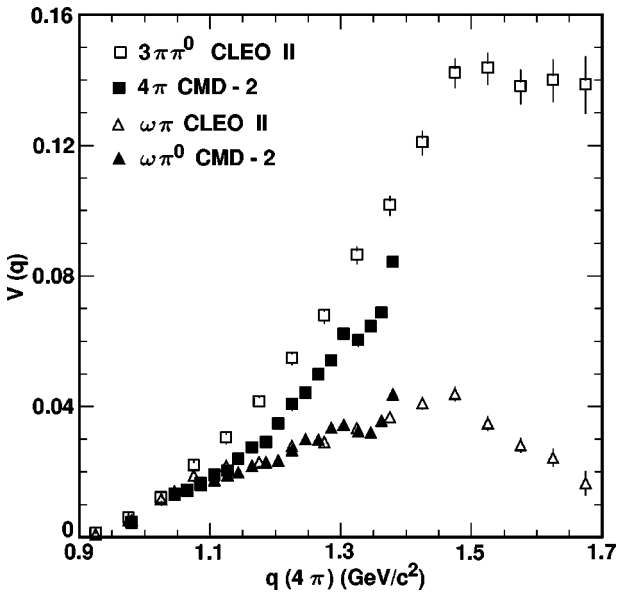

FIG. 12. Comparison of $V^{3\pi\pi^0}(q)$ and $V^{\omega\pi}(q)$ measured in this analysis with the corresponding cross sections measured by CMD-2. Squares represent the full four-pion spectrum, and triangles represent the $\omega\pi$ component. Our results are shown with open symbols, and the results obtained by CMD-2 are shown with filled symbols. Only statistical errors are shown.

H. CVC test

The CVC hypothesis relates the weak charged hadronic current in the τ lepton decay to the isovector part of the electromagnetic current. Thus, the spectral functions $V^{3\pi\pi^0}(q)$ and $V^{\omega\pi}(q)$ can be related [24] to the cross-sections for $e^+e^-\to 4\pi$ as

$$V^{3\pi\pi^0}(q)=\frac{q^2}{4\pi^2\alpha^2}\left[\frac{1}{2}\sigma_{e^+e^-\to 2\pi^+2\pi^-}(q) + \sigma_{e^+e^-\to\pi^+\pi^-2\pi^0}(q)\right], \tag{32}$$

$$V^{\omega\pi}(q)=\frac{q^2}{4\pi^2\alpha^2}\sigma_{e^+e^-\to\omega\pi^0}(q). \tag{33}$$

Therefore, the resonant structure of the hadronic final state in the decay $\tau\to 3\pi\pi^0\nu_\tau$ should be comparable to that in the reactions $e^+e^-\to 2\pi^+2\pi^-$ and $e^+e^-\to\pi^+\pi^-2\pi^0$ in the energy range corresponding to the τ mass. The only expected difference is due to the fact that the $\omega\pi$ final state is not accessible in the all charged final state. A recent analysis of the CMD-2 data [25] shows clear dominance of the $a_1\pi$ component in the four charged pion final state and of the $a_1\pi$ together with the $\omega\pi$ components in the two charged and two neutral pion mode. Our results are in excellent qualitative agreement and support the CVC hypothesis.

A plot comparing the $3\pi\pi^0$ and $\omega\pi$ spectral functions in the decay $\tau\to 3\pi\pi^0\nu_\tau$ with the corresponding cross-sections measured by the CMD-2 group [26] is shown in Fig. 12. Our results for the $\omega\pi$ spectral function are in excellent agreement with the CMD-2 data. The $3\pi\pi^0$ spectral function is about 20% above the recent CMD-2 measurement; this may be explained by a large value of the systematic uncertainty in the CMD-2 measurement: 15%. A compilation [25] of several e^+e^- measurements performed in this energy range also reveals discrepancies between various experimental results that are large enough to account for the difference between our measurement and that of CMD-2. A thorough analysis of the e^+e^- experiments is needed to resolve this problem.

VIII. CONCLUSIONS

The large data sample of $\tau\to 3\pi\pi^0\nu_\tau$ decays collected by the CLEO II experiment allowed for a detailed study of the resonant decomposition and structure functions of the $3\pi\pi^0$ final state. The analysis indicates dominance of the $\omega\pi$ and $a_1\pi$ contributions which is in good agreement with theoretical expectations based on the CVC hypothesis and Chiral Langrangian calculations. At the same time, with the present statistics, other models can provide satisfactory descriptions of the existing resonant structure. The goodness-of-fit is slightly higher for the models with a dominating $a_1\pi$ contribution, though the $a_1\pi$ channel alone does not reproduce the observed non-ω contribution precisely. The mass and width of the ρ' resonance have been extracted from the fit to the $\tau\to\omega\pi\nu_\tau$ spectral function. A new upper limit on the non-vector current contribution to this spectral function of 5.4% at 90% C.L. has been obtained.

ACKNOWLEDGMENTS

We gratefully acknowledge the effort of the CESR staff in providing us with excellent luminosity and running conditions. J.R. Patterson and I.P.J. Shipsey thank the NYI program of the NSF, M. Selen thanks the PFF program of the NSF, M. Selen and H. Yamamoto thank the OJI program of DOE, J.R. Patterson, K. Honscheid, M. Selen and V. Sharma thank the A.P. Sloan Foundation, M. Selen and V. Sharma thank the Research Corporation, F. Blanc thanks the Swiss National Science Foundation, and H. Schwarthoff and E. von Toerne thank the Alexander von Humboldt Stiftung for support. This work was supported by the National Science Foundation, the U.S. Department of Energy, and the Natural Sciences and Engineering Research Council of Canada.

APPENDIX A: HADRONIC CURRENT FOR THE DECAYS $\tau\to a_1\pi\nu_\tau$, $\tau\to\sigma\rho\nu_\tau$, $\tau\to f_0\rho\nu_\tau$, AND $\tau\to\omega\pi\nu_\tau$

Expressions for the hadronic current for τ decays into the four pion final state via $a_1\pi$, $\sigma\rho$, $f_0\rho$, and $\omega\pi$ channels are derived under the assumption that the τ decays into an intermediate vector resonance $\tilde{\rho}$: $\tau\to\tilde{\rho}\nu_\tau$, which consecutively decays into the shown channels. The vector boson $\tilde{\rho}$ has quantum numbers $I(J^{PC})=1(1^{--})$, and its spectral function, in accordance with Eq. (30), is simulated as a mixture of ρ and ρ' resonances and a phase space contribution. Assuming isospin conservation and enforcing Bose symmetry, one obtains the following expressions for the form factors f_i^μ in the decay $\tau^-\to 2\pi^-\pi^+\pi^0\nu_\tau$:

$$f^{\mu}_{a_1\pi} = T^{\mu\nu}(Q)[T_{\nu\kappa}(Q_1)BW_{a_1}(\sqrt{Q_1^2})[BW_{\rho}(\sqrt{(q_3+q_4)^2})(q_3-q_4)^{\kappa} - BW_{\rho}(\sqrt{(q_2+q_3)^2})(q_2-q_3)^{\kappa}]$$

$$+ T_{\nu\kappa}(Q_2)BW_{a_1}(\sqrt{Q_2^2})[BW_{\rho}(\sqrt{(q_3+q_4)^2})(q_3-q_4)^{\kappa} - BW_{\rho}(\sqrt{(q_1+q_3)^2})(q_1-q_3)^{\kappa}]$$

$$- T_{\nu\kappa}(Q_3)BW_{a_1}(\sqrt{Q_3^2})[BW_{\rho}(\sqrt{(q_2+q_4)^2})(q_2-q_4)^{\kappa} + BW_{\rho}(\sqrt{(q_1+q_4)^2})(q_1-q_4)^{\kappa}]], \tag{A1}$$

$$f^{\mu}_{\sigma\rho} = T^{\mu\nu}(Q)[BW_{\sigma}(\sqrt{(q_1+q_4)^2})BW_{\rho}(\sqrt{(q_2+q_3)^2})(q_2-q_3)_{\nu}$$
$$+ BW_{\sigma}(\sqrt{(q_2+q_4)^2})BW_{\rho}(\sqrt{(q_1+q_3)^2})(q_1-q_3)_{\nu}], \tag{A2}$$

$$f^{\mu}_{\omega\pi} = BW_{\omega}(\sqrt{Q_2^2})[q_1^{\mu}[(Q_2\cdot q_3)(q_2\cdot q_4) - (Q_2\cdot q_4)(q_2\cdot q_3)] + q_3^{\mu}[(Q_2\cdot q_4)(q_1\cdot q_2) - (q_1\cdot Q_2)(q_2\cdot q_4)]$$

$$+ q_4^{\mu}[(q_1\cdot Q_2)(q_2\cdot q_3) - (Q_2\cdot q_3)(q_1\cdot q_2)]] + (1 \leftrightarrow 2), \tag{A3}$$

where

$$\begin{aligned} q_1 &:= \text{four-momentum of} \quad \pi_1^-, \\ q_2 &:= \text{four-momentum of} \quad \pi_2^-, \\ q_3 &:= \text{four-momentum of} \quad \pi^0, \\ q_4 &:= \text{four-momentum of} \quad \pi^+, \end{aligned} \tag{A4}$$

$$\begin{aligned} Q &= q_1 + q_2 + q_3 + q_4, \\ Q_1 &= q_2 + q_3 + q_4, \\ Q_2 &= q_1 + q_3 + q_4, \\ Q_3 &= q_1 + q_2 + q_4, \end{aligned} \tag{A5}$$

and $T^{\mu\nu}(x)$ denotes the projection operator:

$$T^{\mu\nu}(x) = -g^{\mu\nu} + \frac{x^{\mu}x^{\nu}}{x^2}. \tag{A6}$$

The expression for the τ decay into four pions via the $f_0\rho$ channel is identical to Eq. (A2) with the mass of f_0 substituted instead of the mass of σ.

[1] ARGUS Collaboration, H. Albrecht *et al.*, Phys. Lett. B **185**, 223 (1987).
[2] CLEO Collaboration, P. Baringer *et al.*, Phys. Rev. Lett. **59**, 1993 (1987).
[3] ARGUS Collaboration, H. Albrecht *et al.*, Phys. Lett. B **260**, 259 (1991).
[4] ALEPH Collaboration, D. Buskulic *et al.*, Z. Phys. C **74**, 101 (1997).
[5] J. H. Kuhn and A. Santamaria, Z. Phys. C **48**, 445 (1990).
[6] J. H. Kuhn and E. Mirkes, Z. Phys. C **56**, 661 (1992).
[7] R. Decker and E. Mirkes, Z. Phys. C **57**, 495 (1993).
[8] B. A. Li, Phys. Rev. D **58**, 097 302 (1998).
[9] S. I. Eidelman and V. N. Ivanchenko, Nucl. Phys. B (Proc. Suppl.) **55C**, 181 (1997).
[10] Particle Data Group, C. Caso *et al.*, Eur. Phys. J. C **3**, 1 (1998).
[11] ALEPH Collaboration, R. Barate *et al.*, Z. Phys. C **76**, 15 (1997).
[12] J. Urheim, Nucl. Phys. B (Proc. Suppl.) **55C**, 359 (1997).
[13] S. Weinberg, Phys. Rev. **112**, 1375 (1958).
[14] CLEO Collaboration, Y. Kubota *et al.*, Nucl. Instrum. Methods Phys. Res. A **320**, 66 (1992).
[15] CLEO Collaboration, J. Alexander *et al.*, Phys. Rev. D **56**, 5320 (1997).
[16] Y. S. Tsai, Phys. Rev. D **4**, 2821 (1971).
[17] S. I. Dolinsky, Phys. Lett. B **174**, 453 (1986).
[18] S. U. Chung, O. I. Dahl, J. Kirz, and D. H. Miller, Phys. Rev. **165**, 1491 (1968).

[19] KORALB (v. 2.1), S. Jadach and Z. Was, Comput. Phys. Commun. **36**, 191 (1985); **64**, 267 (1991); **85**, 453 (1995); TAUOLA (v. 1.5), S. Jadach, J. H. Kühn, and Z. Was, *ibid.* **64**, 275 (1991); **70**, 69 (1992); **76**, 361 (1993)..
[20] R. Decker, Z. Phys. C **36**, 487 (1987).
[21] R. Decker *et al.,* Z. Phys. C **70**, 247 (1996).
[22] R. Fisher, J. Wess, and F. Wagner, Z. Phys. C **3**, 313 (1980).
[23] N. A. Törnqvist, Z. Phys. C **68**, 647 (1995).
[24] F. J. Gilman and D. H. Miller, Phys. Rev. D **17**, 1846 (1978); F. J. Gilman and S. H. Rhie, *ibid.* **31**, 1066 (1985).
[25] R. R. Akhmetshin *et al.*, hep-ex/9904024, 1999.
[26] A. E. Bondar *et al.*, hep-ph/9907283, 1999.